

Experimental test of Landauer’s principle for stochastic resetting

Rémi Goerlich,^{1,2,*} Minghao Li,^{3,4} Luis B. Pires,² Paul-Antoine Hervieux,¹ Giovanni Manfredi,¹ and Cyriaque Genet²

¹Université de Strasbourg, CNRS, Institut de Physique et Chimie des Matériaux de Strasbourg, UMR 7504, F-67000 Strasbourg, France

²Université de Strasbourg, CNRS, Centre Européen de Sciences Quantiques & Institut de Science et d’Ingénierie Supramoléculaires, UMR 7006, F-67000 Strasbourg, France

³Department of Physics, University of Basel, Klingelbergstrasse 82, 4056 Basel, Switzerland

⁴Swiss Nanoscience Institute, Klingelbergstrasse 82, 4056 Basel, Switzerland

(Dated: June 19, 2023)

A diffusive process that is reset to its origin at random times, so-called stochastic resetting (SR) is an ubiquitous expedient in many natural systems [1]. Beyond its ability to improve efficiency of target searching, SR is a true non-equilibrium thermodynamic process that brings forward new and challenging questions [2]. Here, we experimentally implement SR within a time-dependent optical trapping potential and give a quantitative assessment of its thermodynamics. We show in particular that SR operates as a Maxwell demon, converting heat into work from a single bath continuously and without feedback [3, 4]. Such a demon is the manifestation of the constant erasure of information at play in resetting that, in our experiments, takes the form of a protocol. By tailoring this protocol, we can bring the demon down to its minimal energetic cost, the Landauer bound [5]. In addition, we reveal that the individual trajectories forming this autonomous demon all break ergodicity and thereby demonstrate the non-ergodic nature of the demon’s *modus operandi*.

In a stochastic resetting (SR) process, a Brownian object diffuses, either freely or in a potential, for a random time τ before being reset to the origin [1, 6–8]. This simple yet rich paradigm has drawn a lot of attention recently in various fields of research. Because it minimizes first passage times in search process [9] SR is the adequate solution to numerous search problems in nature [10, 11] and in algorithms used for instance in molecular dynamics [12]. Thermodynamically, resetting brings the system in a non-equilibrium steady state with specific properties. Consequently, the ability to improve efficiency of target searching comes with a cost that has to be balanced with the gain in search time [2, 13]. Such a complex trade-off is embedded in natural processes relying on resetting, but its quantitative characterization is still missing. This is currently not only driving intense theoretical efforts related to the thermodynamic cost associated to resetting [14–18] but is also challenging experimentalists to fill-in the gap between an idealized, theoretical SR process and its actual physical realization. We note that this cost has an informational nature, since each resetting event, in an idealized framework, is an instantaneous erasure of a finite amount of information. Remarkably, the corresponding thermodynamics can be quantified when resetting happens in a confining potential, where heat is effectively absorbed from a single heat bath and work extracted [2]. Such a Maxwell demon is constrained by a non-equilibrium second law, imposing a bound on the minimal amount of energy that has to be fed into the system, at least equal to the extracted work [4, 19]. However, a physical implementation of SR necessarily involves continuous trajectories, that consume a larger amount of energy. To test the bound derived from the second law and extract its informational significance, the thermodynamic description has therefore to be adjusted to such a real situation. Doing so, we can show that the information thermodynamics of SR is rooted in

the irreversibility of the process imprinted at the level of each individual stochastic trajectories. By measuring from all such trajectories the non-ergodic nature of SR, we further stress the link between ergodicity breaking and information processing [20–22].

Experimentally, an SR process can be implemented through various ways [23, 24]. Here, we set up a platform where it is possible to discuss, from the same trajectories, both the real and idealized situations, with their respective thermodynamic descriptions. This platform consists of a Brownian microsphere subjected to a time-dependent optical potential with two states: (i) a weak potential state, allowing the microsphere to diffuse during a time τ and (ii) a strongly confining state, quenching the particle very close to $x = 0$ and resetting its position in a waiting time τ_w . We choose to reset the microsphere’s trajectory randomly in time with a constant rate λ , hence implementing within our optical trap a Poissonian SR process. Our experimental method is similar to the one proposed in [25] and used in [24, 26] but differs from [23].

Our capacity to record real-time trajectories allows us to handle both the idealized SR process (by removing the waiting times τ_w) and the actual physical process implemented in the trap (by keeping the whole time-series). For the idealized case, all appropriate thermodynamic quantities can be measured in particular the non-equilibrium free energy difference Δf of resetting evaluated on one single resetting event, *i.e.* the instantaneous jump from a random position x_t to a deterministic reference $x = 0$. From this, the non-equilibrium second laws can be derived and the features of the Maxwell demon quantified. In parallel, the full thermodynamic cost of our physical platform is assessed by applying to the full Langevin trajectories including waiting times the methods of stochastic energetics [27]. We will show below that the total work W_{ext} externally needed to maintain the system in its non-equilibrium steady state is bounded by this non-equilibrium free energy difference Δf . Involving full trajectories, W_{ext} depends on the actual protocol used to reset, in sharp contrast with the bound Δf , that only depends on the resetting

* Present address: Raymond & Beverly Sackler School of Chemistry, Tel Aviv University, Tel Aviv 6997801, Israel

parameters. Our experiment allows us to approach this ideal bound, by slowing down each individual resetting event, at a constant resetting rate. By considering resetting as an erasure process necessarily accompanied by a loss of information, the energetic bound is endowed with an informational dimension: the Landauer's limit. In the real system, the physical work W_{ext} can be pushed down to this limit by smoothing each resetting event towards a quasistatic protocol. Fundamentally, erasing information necessarily implies a breaking of ergodicity that we do observe on the recorded trajectories. It is a clear asset of our experimental platform to be able to reveal, in a straightforward way, the profound connections between the non-equilibrium second law, erasure of information and ergodicity breaking.

Our experimental setup (sketched on Fig. 1, upper panel and detailed in Appendix A) consists of a $3\ \mu\text{m}$ polystyrene sphere diffusing in a fluidic cell filled with water at ambient temperature $T = 296\ \text{K}$. A laser beam (820 nm, CW) is focused through a high numerical aperture objective onto the fluidic cell in order to induce a harmonic optical potential in the vicinity of the focal waist. A secondary low-power laser beam acts as a passive probe, allowing to record in real-time the position x_t of the microsphere (throughout the paper, x_t refers to the stochastic position at time t while x is the standard space variable). The stiffness κ of the harmonic confinement is linearly related to the intensity of the trapping beam controlled numerically (see details in Appendix A). If the stiffness of the optical trap is low $\kappa = \kappa_{\text{min}}$, the particle explores a shallow potential, with diffusion coefficient $D = k_B T / \gamma$ given by Boltzmann constant k_B , temperature T and Stokes drag coefficient γ and with relaxation time $\omega_0^{-1} = \gamma / \kappa_{\text{min}}$. When the stiffness abruptly increases to a high value $\kappa = \kappa_{\text{max}}$ (typically $\kappa_{\text{max}} \approx 100\ \kappa_{\text{min}}$), the particle relaxes exponentially fast towards the center of the potential $x = 0$, with a characteristic relaxation time $\omega_{\text{max}}^{-1} = \gamma / \kappa_{\text{max}}$. This stiffness quench can be interpreted as a resetting event and to ensure that the particle is well reset, the potential is kept stiff for a waiting time τ_w several times larger than the relaxation time. There, the remaining fluctuations of the microsphere around $x = 0$ are as small as $\sqrt{k_B T / \kappa_{\text{max}}}$ *i.e.* a few nanometers with typical experimental values.

In the specific case of Poissonian SR, the duration τ of each diffusive period where $\kappa = \kappa_{\text{min}}$ is a random variable drawn out of an exponential distribution $P_r(\tau) = \lambda e^{-\lambda\tau}$ with rate λ , before κ is quenched to κ_{max} . This realization of SR cannot depart from an ideal theoretical resetting process due to the non-instantaneous nature of the relaxation to $x = 0$ (studied in [17, 28–30]). But an ideal SR process can be recovered if one removes from the experimental data the transient times τ_w when the microsphere is relaxing in the optical trap [31], obtaining an instantaneous resetting. This is exactly what our experimental platform allows.

On Fig. 1 (top panel), we show an experimentally recorded SR process in a potential $V(x) = \kappa_{\text{min}} x^2 / 2$ with $\kappa_{\text{min}} = 3.15 \pm 0.13$, $\kappa_{\text{max}} = 97 \pm 4.2\ \text{pN}/\mu\text{m}$ with an inverse resetting rate $\lambda^{-1} = 1.5\ \text{ms}$. The trajectory is recorded for 300 seconds at a frequency $2^{15} = 32768\ \text{Hz}$. As explained above, the

points during waiting times τ_w are removed to approach an ideal instantaneous SR process. Importantly, the removing of these sections in the time-series erase the memory of the trajectory: there is no correlations between the position before and after each resetting event since $\tau_w > \omega_{\text{max}}^{-1}$. The resetting events are marked by red arrows on Fig. 1 (top panel) and the non-exact resetting position is underlined by a red stripe around $x = 0$.

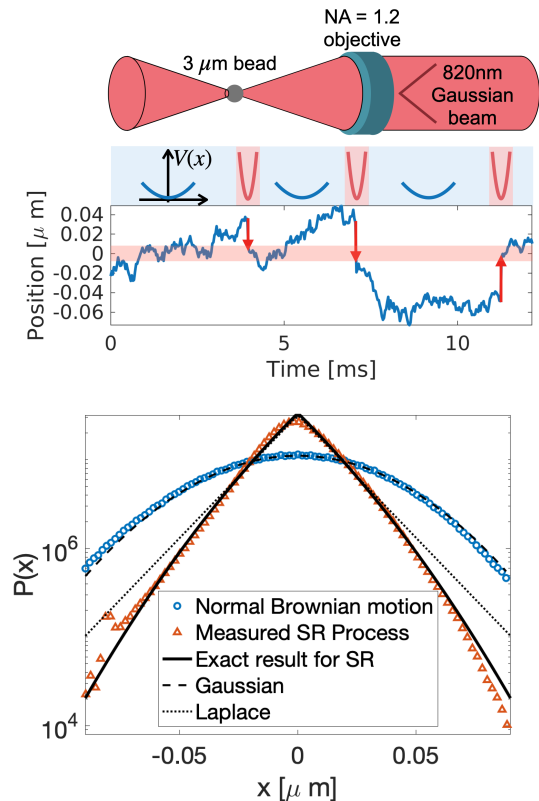


FIG. 1. (Upper panel) Simplified view of the optical trapping system: a 820 nm laser beam, tightly focused through a high numerical aperture objective is confining the motion of a $3\ \mu\text{m}$ polystyrene bead in water. (Middle panel) Experimental trajectory of the bead diffusing in a potential $V(x) = \kappa_{\text{min}} x^2 / 2$ (depicted above the trajectory as a blue line), subjected to stochastic resetting (through potential quenches, depicted above the trajectory as a red line) at a rate $\lambda = 662\ \text{Hz}$. Resetting events towards $x = 0$ are marked on the trajectory with red arrows. As detailed in the main text, this instantaneous SR process is built from a recorded trajectory subjected to a time-dependent optical potential by removing the data recorded during the waiting times when the stiffness is κ_{max} (see Appendix A for experimental details). (Lower panel) Probability distribution of position $P(x)$ of a 300 seconds-long SR process (red triangles) with rate λ in potential $V(x)$ together with the exact result derived in Appendix D, with experimental parameters (black solid line). The equilibrium distribution $P_{\text{eq}}(x)$ of a normal Ornstein-Uhlenbeck process in the potential $V(x)$ (blue circles) is a Gaussian (black dashed line) as expected for trapped Brownian object. The SR probability distribution $P(x)$ significantly differs both from $P_{\text{eq}}(x)$ and from the Laplace distribution of a free SR process [1] (black dotted line) showing the combined effect of resetting and confining potential $V(x)$.

Our experimental SR reaches a steady-state distribution

$P(x)$ that can be compared with an exact result for SR in a quadratic potential [32]. The distribution, computed as $P(x) = \lambda \int_0^\infty e^{-\lambda t} G(x|t, x=0) dt$ gives the probability for the particle to diffuse from 0 to x in a time t [18]. Here, $G(x|t, x=0)$ is the standard Ornstein-Uhlenbeck propagator for Brownian diffusion within a potential. We derive in Appendix D the exact steady-state distribution that generalizes to real values of the λ/ω_0 ratio the known expression for SR in a harmonic potential [33].

On Fig. 1 (lower panel), we plot the probability distributions built from these decimated trajectories. The agreement between the experimental non-equilibrium steady-state (red triangles) and the analytical result validates the experimental method and confirms that the decimated experimental trajectories are very close to those of an ideal SR process. The agreement also shows that the experimental error on the resetting position (red stripe on the upper panel) can be neglected and that the system can be described as an ideal SR process in a potential. On the same graph, we plot in blue the equilibrium distribution of the normal Ornstein-Uhlenbeck process without resetting. This diffusion in the harmonic potential $V(x)$ is characterized by a Gaussian distribution $P_{\text{eq}}(x) = \sqrt{\frac{\kappa_{\text{min}}}{2\pi k_B T}} e^{-\kappa_{\text{min}} x^2 / 2k_B T}$. It is clear that the SR process, confining the motion inside the trap, reaches a distribution that strongly differs from the equilibrium Gaussian density of Brownian diffusion in the harmonic potential $V(x)$.

Bringing the system into a non-equilibrium steady-state (NESS), the SR process necessarily consumes and dissipates energy, both in the ideal case and in the experimental implementation. For an ideal SR and on the level of single stochastic trajectories, each resetting event is an abrupt change in the potential energy of the system from $V(x_t)$ to $V(0)$. This formally corresponds to a stochastic work $\Delta w = V(x_t) - V(0)$ exerted against the external potential. Each resetting event also implies a change in stochastic Shannon entropy $\Delta s = s(x_t) - s(0) = k_B \ln[P(x_t)/P(0)]$ [34]. Therefore, resetting is characterized by a stochastic change in non-equilibrium free energy expressed as $\Delta f = \Delta w - T\Delta s$ [19]. Importantly, this quantity is universally valid for any SR process in an energy landscape $V(x)$, but defined for an instantaneous resetting [2, 14–16].

For our experiments, the energetics of SR can be precisely described within the appropriate framework where the work, applied on the system when performing the quench in the trapping stiffness, can be precisely evaluated, as we detail below. A central result of our work is the experimental demonstration that the external power needed to maintain the system in this NESS is bounded from below by the average non-equilibrium free energy [19]

$$\dot{W}_{\text{ext}} \geq \lambda \langle \Delta f \rangle, \quad (1)$$

where $\langle \dots \rangle$ denotes the ensemble average $\int \dots P(x) dx$ performed over the resetting jumps ($x_t, x=0$). The right-hand-side of this equation corresponds to an universal quantity, in the sense that it is independent of the specific method used to reset. On our platform, it can be evaluated experimentally,

simply by removing the waiting times τ_w from the trajectories the idealized scheme described above. In contrast, the left-hand-side term depends on the precise protocol used to reset the particle, as analyzed further down. It can also be evaluated on our platform but this time looking at the whole trajectories subjected to a time-dependent potential using the methods of stochastic energetics. One key advantage of our approach is the possibility to measure both \dot{W}_{ext} and $\lambda \langle \Delta f \rangle$ thermodynamic quantities and hence to probe Eq. (1) as a central experimental constraint.

Removing the waiting times enables a full energetic analysis of the idealized SR process that reveals the Maxwell demon nature of the system. Importantly, specific entropic relations will emerge from this analysis that will set bounds on any physical implementation of SR in the form of a non-equilibrium second law of thermodynamics.

The mean free energy cost of ideal resetting is obtained by multiplying the stochastic free energy change Δf by the resetting rate λ and performing the ensemble average as

$$\lambda \langle \Delta f \rangle = \lambda \langle V(x_t) \rangle - k_B T \lambda \left\langle \ln \left[\frac{P(x_t)}{P(0)} \right] \right\rangle, \quad (2)$$

accounting for $V(0) = 0$ in the harmonic regime. The first term in this expression is the average rate of extracted work $\dot{W} = \lambda \langle V(x_t) \rangle$, which is always positive. It is accompanied by a heat dissipation due to the non-vanishing probability current $j(x) = (-\frac{1}{\gamma} \frac{dV(x)}{dx} - D\partial_x)P(x)$ maintaining the NESS distribution different from the equilibrium solution P_{eq} in the external potential. Since the current can be evaluated using the experimental distribution $P(x)$ of the recorded trajectories, the dissipated heat given by $\dot{Q} = \int j(x) \frac{dV(x)}{dx} dx$ can be experimentally measured [2]. Since in the idealized framework, the external potential is constant, there is no change in internal energy. As a direct thermodynamic consequence, the first law for resetting reads $\dot{Q} + \dot{W} = 0$.

On Fig. 2 (top panel), we display the heat and work production rates evaluated on our experimentally idealized SR process, as a function of the mean resetting time λ^{-1} , while keeping the same κ_{min} and κ_{max} . The experimental results are complemented by numerical simulations (see Appendix B for details). The sum $\dot{Q} + \dot{W}$ vanishes for all resetting rates as expected from the first principle of thermodynamics. Remarkably, $\dot{Q} < 0$ for all probed λ^{-1} : heat is effectively absorbed from the heat bath at a single constant temperature and work is extracted. This blatantly shows that SR in a confining potential emulates a true Maxwell demon, confirming the prediction of [2].

The second term in the non-equilibrium free energy (2) is proportional to the average rate of stochastic Shannon entropy change Δs . The mean resetting entropy production rate is obtained by averaging Δs over resetting events:

$$\dot{S}^{\text{rst}} = \lambda \langle \Delta s \rangle = k_B \lambda \int \ln \left[\frac{P(x_t)}{P(0)} \right] P(x) dx. \quad (3)$$

This quantity does not account for the contribution of the diffusive trajectory between resetting. This contribution enters

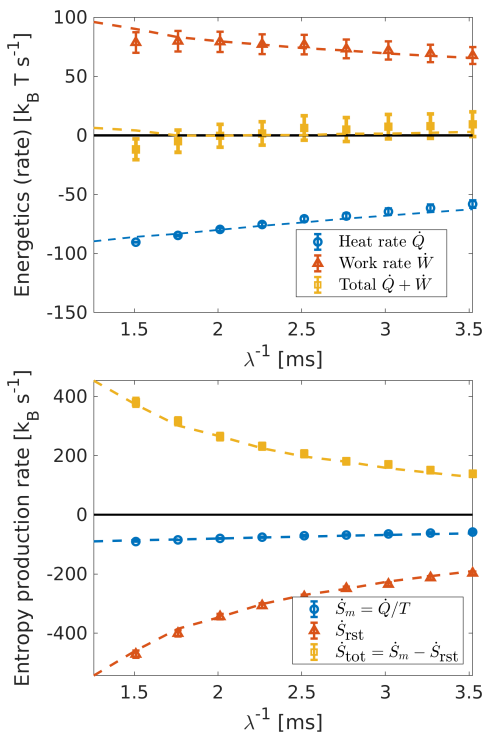


FIG. 2. (Upper panel) Experimentally measured work production rates \dot{W} and heat production rates \dot{Q} for an SR process with inverse resetting rates λ^{-1} ranging from 1.5 to 3.5 milliseconds. Their vanishing sum for all λ demonstrates the first law of thermodynamics for resetting. The experimental data are compared with numerical simulations (dotted lines) in the same conditions. A minor calibration error is corrected by comparing a measured variance with a numerical result (see Appendix B). (Lower panel) Second law of thermodynamics for the same inverse resetting rates λ^{-1} . The medium entropy production rate, given by the heat dissipation divided by temperature, as explained in the main text. The resetting entropy production rate, as explained in the main text. The total entropy production rate $\dot{S}^{\text{tot}} = \dot{S}^{\text{m}} - \dot{S}^{\text{rst}}$ is a positive quantity for all λ as expected from the second law of thermodynamics [2]. The negativity of \dot{Q} and \dot{S}^{m} shows that the system constantly extracts heat from the reservoir in order to stay in the non-equilibrium state $P(x)$, operating as a Maxwell demon.

in the heat production rate, to which is associated a dissipation of entropy in the medium, $\dot{S}^{\text{m}} = \dot{Q}/T$. Finally, the total entropy production rate of a Brownian trajectory experiencing SR reads $\dot{S}^{\text{tot}} = \dot{S}^{\text{m}} + \dot{S}^{\text{sys}} - \dot{S}^{\text{rst}} \geq 0$, as derived in [17]. The system entropy $\dot{S}^{\text{sys}} = k_B \frac{d}{dt} \int P(x) \ln[P(x)] dx$ vanishes in the steady-state [15, 35]. Therefore, here, the total entropy production rate

$$\dot{S}^{\text{tot}} = \dot{S}^{\text{m}} - \dot{S}^{\text{rst}} \geq 0 \quad (4)$$

is a positive quantity, only reaching zero in the limit of equilibrium. As such, it is interpreted as the second law of thermodynamics for an SR process [2, 18, 19]. On Fig. 2, we show both entropy production rates as well as \dot{S}^{tot} , which remains, as expected, a positive quantity. \dot{S}^{tot} decreases with λ^{-1} , experimentally verifying this non-equilibrium second law of thermodynamics for stochastic resetting. The limit of long λ^{-1}

corresponds to the absence of resetting, recovering an equilibrium dynamics.

With Eq. (4), the thermodynamic content of the ideal SR free energy can be further specified with $\lambda \langle \Delta f \rangle = \dot{W} - T \dot{S}^{\text{rst}}$. As we stressed already above, $\lambda \langle \Delta f \rangle$ only depends on the resetting rate and on the potential in which diffusion occurs but does not depend on how resetting is performed. This dependence can be quantified by evaluating the external work actually involved for driving the potential through a sequence of successive resetting events, see Eq. (1)

To do so, the full trajectories, including the waiting times τ_w are analyzed as Langevin trajectories that experience a time-dependant potential. In our experiment, the choice of the individual protocol $\kappa(t)$ connecting κ_{min} and κ_{max} to implement resetting will change the response of the microsphere and induce a different energy exchange. In the framework of stochastic energetics, the work is computed as [17, 27]

$$W^{\text{ext}}(t) = -\frac{1}{2} \int_0^t \dot{\kappa}(t') x_t^2 dt' \quad (5)$$

and the averaged work production rate on a long trajectory of length $t_{\text{tot}} \gg \lambda^{-1}$ (containing many resetting events) is simply $\dot{W}^{\text{ext}} = W^{\text{ext}}(t_{\text{tot}})/t_{\text{tot}}$. This external applied work obviously depends on the choice of $\kappa(t)$ connecting the same initial κ_{min} and final κ_{max} stiffnesses at the same rate λ . This protocol-dependence of \dot{W}^{ext} needed to maintain SR sheds an original light on $\lambda \langle \Delta f \rangle$ that can be interpreted as a Landauer's bound, as we now show.

We start by designing smooth protocols for similar resetting sequence at a given rate λ , but where each increase in stiffness for resetting is obeying $\kappa(t) = (\kappa_{\text{max}} - \kappa_{\text{min}}) \tanh\left(\frac{t}{\epsilon}\right) + \kappa_{\text{min}}$. This allows us to perform SR with protocols ranging from abrupt step-like changes for small ϵ to slow drivings for large $\epsilon \gg \omega_{\text{max}}^{-1}$, thus approaching the quasistatic limit.

The different protocols applied between $\kappa_{\text{min}} = 2.2 \pm 0.12$ and $\kappa_{\text{max}} = 95 \pm 4.7$ pN/ μm and ranging from a step-like protocol to a smooth transition are displayed on Fig. 3 (upper panel). For each, we record a long time-series of positions x_t and measure the associated \dot{W}^{ext} as well as the free energy $\lambda \langle \Delta f \rangle = \dot{W} - T \dot{S}^{\text{rst}}$. These energetics are plotted on Fig. 3 (lower panel) where we can notice that $\lambda \langle \Delta f \rangle$ is, as expected, independent on the choice of $\kappa(t)$. Strikingly, we observe that the external work is always larger than this constant non-equilibrium free energy and that it approaches it asymptotically as ϵ increases for slower protocols. This clearly demonstrates the bounding role of the free-energy cost of the ideal SR process with respect to the external energy needed to experimentally perform SR, as expressed by Eq. 1. These results evidently underline the major difference between an idealized process and its physical implementation.

Let us now turn to the informational nature of SR. In SR, the instantaneous jump from a stochastic position towards the center of the potential (with a full loss of correlation with the past trajectory) effectively erases the information stored in the random position x_t . From this perspective, our experimental results endow this bound with a new significance in which the constant $\lambda \langle \Delta f \rangle$ corresponds to the Landauer's limit [36, 37]. We stress that it is through experiments that we are able to

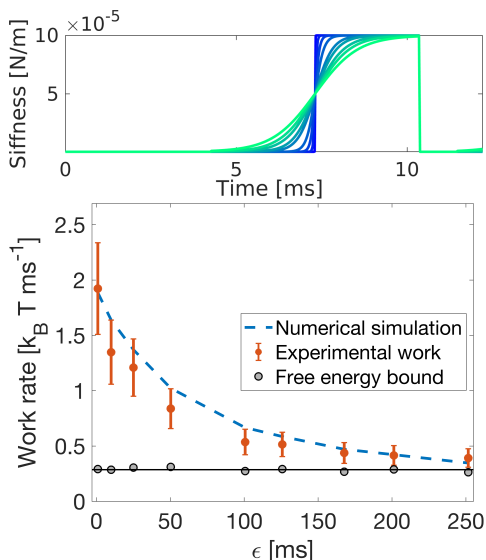


FIG. 3. (Upper panel) Different protocols $\kappa(t)$ for a single resetting event connecting the same κ_{\min} and κ_{\max} . The parameter ϵ governs the shape of the protocol, ranging from a very abrupt step-like protocol with $\epsilon = 1$ ms (blue line), to a very slow close-to-quasistatic hyperbolic tangent protocol for a large $\epsilon = 250$ ms (green line). The relaxation time of the particle in the external potential is $\omega_0^{-1} = \gamma/\kappa_{\min} = 11.5$ ms (the relaxation time in the stiff resetting potential is $\omega_{\max}^{-1} = \gamma/\kappa_{\max} = 0.26$ ms). Each class of protocol is then used for every individual resetting event of a long SR process. Hence, in each case, the recorded trajectory experiences SR with the exact same parameters κ_{\min} , κ_{\max} and λ , the only difference being the abruptness of every single potential quench. (Lower panel) Associated stochastic work (red circles) experimentally measured with Eq. (5), applying the standard tools of stochastic thermodynamics to the full trajectory under time-dependant potential. Landauer's limit set by the free energy $\dot{W} - T\dot{S}^{\text{rst}}$ measured on the ideal instantaneous resetting process (black circles and black solid line) is approached for large ϵ , when each resetting event is closer to the quasistatic limit. The experimental data are in good agreement with numerical simulations (blue dashed line) performed in the same conditions.

probe both ideal and real situations and quantitatively characterize the thermodynamics at play in the SR process down to its fundamental Landauer's bound.

We finally discuss another essential, yet seldom analyzed, aspect of SR. For a system to operate with information and memory, ergodicity must be broken on the time scale of the experiment [38]. In the classical example of a 2-state memory, non-ergodicity is the condition for micro-states to become distinguishable and on which information can be stored or erased [36]. In the case of resetting, memory erasure takes place with the instantaneous jumps towards the resetting position, visible only at the level of stochastic trajectories [39]. The presence of these jumps breaks micro-reversibility and ergodicity by the same mechanism [22]. Landauer's bound Eq. (1) setting the minimal cost of operating SR is therefore closely connected to the non-ergodic nature of the stochastic trajectories. In this section we will use a strong ergodic criterion to demonstrate the non-ergodic nature of the SR pro-

cess recorded on our platform while verifying the ergodicity of a normal Brownian diffusion without resetting.

For stationary processes, ergodicity is defined as the equality of time average and ensemble average in the limit of infinite time and infinitely large ensemble. This definition can be given an operational form by applying it on the Mean-Squared-Displacement (MSD) of the Brownian trajectory. Indeed, for a centered stationary process, the MSD is the first non-trivial moment and the convergence on a statistical ensemble of its time-average and ensemble-average is a measure of the ergodic nature of the process [40, 41].

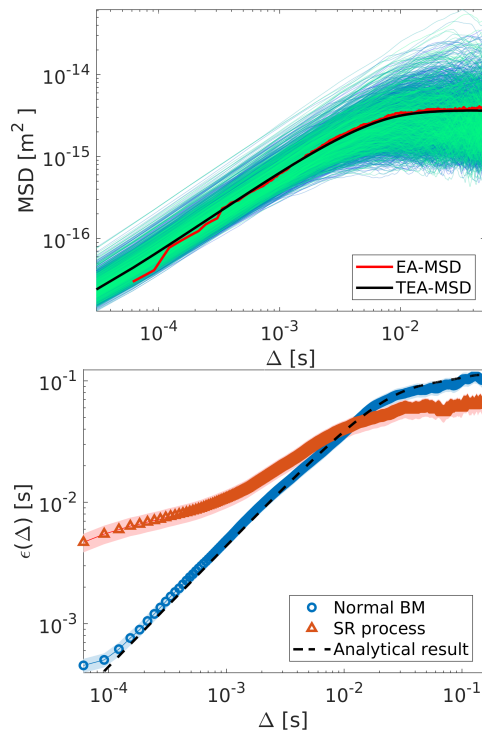


FIG. 4. (Upper panel) Time-averaged-MSDs (TA-MSD) of an ensemble of 800 individual sub-trajectories (light lines from blue to green) together with the instantaneous ensemble-averaged MSD (EA-MSD, red solid line). Averaging again all the TA-MSDs over the ensemble leads to the TEA-MSD (black solid line), which coincides with the EA-MSD. Importantly, the dispersion of TA-MSDs is due to the intrinsic variability of individual sub-trajectories (as explained in the main text), revealing the non-ergodicity of the process. (Lower panel) Ergodic criteria $\epsilon(\Delta)$ quantifying the dispersion of TA-MSDs both for an equilibrium Brownian motion (BM) in the potential $V(x)$ without resetting (normal BM, blue circles) and an SR process in the same potential (red triangles). The analytical expression for $\epsilon(\Delta)$ (black dashed line) coincides with the experimental result for normal BM while the measured values for an SR process are significantly different. This demonstrates that, while the dispersion of TA-MSD for a normal Brownian motion is due solely to the finite statistics of the experiment, the dispersion of TA-MSD for the SR process is induced by an intrinsic variability of sub-trajectories, breaking the ergodicity of the ensemble. Long time drift in the experimental setup had to be corrected with a method detailed in Appendix C.

In our case where the SR process reaches a steady state,

such an ensemble can be built by cutting the long recorded trajectory into shorter sub-trajectories. Here we study an SR process with $\kappa_{\min} = 2.9 \pm 0.15$ and $\kappa_{\max} = 83 \pm 2.1$ pN/ μm at a rate $\lambda^{-1} = 20 \times \gamma/\kappa_{\max} \approx 6.1$ ms. We also verify ergodicity of a normal Brownian motion in exactly the same $V(x)$ external harmonic potential. After removing the waiting times, we obtain a 239 seconds-long SR trajectory that is cut into an ensemble of 800 individual trajectories of a total time $\mathcal{T} = 0.3$ seconds so that each individual sub-trajectory contains many resetting events. On this ensemble, a time-averaged MSD (denoted as TA-MSD) can be computed for each individual i^{th} trajectory as

$$\text{TA-MSD}_i \equiv \overline{\delta x^{i2}(\Delta)} \equiv \frac{1}{\mathcal{T} - \Delta} \int_0^{\mathcal{T} - \Delta} (x_{t+\Delta}^i - x_t^i)^2 dt \quad (6)$$

where \mathcal{T} is the total time of the measured sub-trajectory x_t^i . On the other hand, an instantaneous ensemble-averaged MSD $\langle \delta x^{i2}(\Delta) \rangle$ (denoted as EA-MSD) can be computed on the whole ensemble, by summing over trajectories instead of integrating over time. Finally, both averaging can be combined and the set of individual TA-MSD $_i$ can be averaged on the ensemble to build the time-ensemble averaged MSD (denoted as TEA-MSD).

As discussed in details in our previous work [42, 43], a first necessary condition for ergodicity is the convergence of TEA-MSD to the EA-MSD in the limit of large \mathcal{T}/Δ . This is verified on Fig. 4 (top panel) where we see that the TEA-MSD is superimposed with the EA-MSD. However, this is only a necessary condition for ergodicity since it can hide a strong dispersion of individual TA-MSD $_i$ (which is also visible on Fig. 4 with individual curves from blue to green), implying that individual sub-trajectories strongly differ from each other, violating the ergodic condition. Therefore, a strong ergodicity criterion (both necessary and sufficient condition) is the vanishing of the dispersion of TA-MSD $_i$ in the large \mathcal{T}/Δ limit.

This dispersion of individual TA-MSD is well captured by the estimator $\epsilon(\Delta) = \left\langle \frac{\overline{\delta x^{i2}(\Delta)^2}}{\langle \overline{\delta x^{i2}(\Delta)} \rangle^2} \right\rangle - 1$ that can be analytically computed for normal Brownian motion [43, 44]. The estimator is evaluated on Fig. 4 (lower panel) both for a normal Brownian motion (blue circles) and the SR process (red triangles) in the same potential $V(x)$. We clearly see the non-ergodic nature of SR from the behavior of $\epsilon(\Delta)$, that does not go to zero for short Δ , in agreement with previous numerical works [22]. This demonstrates the non-ergodicity of SR trajectories over all probed time-scales. In contrast, the evolution of $\epsilon(\Delta)$ in the short Δ limit for normal Brownian motion in the same external potential ensures the ergodicity of the experimental setup when no resetting is performed. These two results show that resetting is the sole mechanism breaking ergodicity. Combined with the thermodynamic analysis of above, these results clearly underline the link between ergodicity breaking and the ability to process information and hence the capacity of our system to perform as a Maxwell demon [38].

In this work, we used a simple optically trapped microsphere to implement a stochastic resetting process within a

potential. The recorded trajectories were analyzed through the prism of both thermodynamics and ergodicity. Importantly, the same trajectories were used to explore both an ideal, instantaneous resetting process which has a clear informational nature, and a real, specific experimental realization analyzed with the tools of stochastic energetics. From the recorded non-equilibrium trajectories, we measured the free energy of the system and tested experimentally both the first and second laws of thermodynamics in a resetting context. These tests clearly revealed the Maxwell demon nature of the SR process, indicating that the performance of resetting must be limited by an informational bound. Remarkably, each resetting event corresponds to an erasure process defined in our experiments from a control parameter that follows a specific protocol. This led us to devise and implement a test of Landauer's bound for the minimal work that needs to be applied on the system for it to work as a demon. By engineering slow resetting protocols, we were able to reach experimentally the limit put on the minimal power needed to feed a physical SR system. By combining in our simple experimental scheme the thermodynamics of information with the stochastic dynamics of microscopic trajectories, we have finally verified the connection between the capacity to process information and the breaking of ergodicity. This fundamental connection opens promising perspectives, where ergodicity breaking could serve as a quantitative evaluation and measure of the non-equilibrium properties of information engines.

ACKNOWLEDGMENTS

We sincerely thank Yael Roichman and Shlomi Reuveni for discussions. This work is part of the Interdisciplinary Thematic Institute QMat of the University of Strasbourg, CNRS and Inserm. It was supported by the following programs: IdEx Unistra (ANR-10-IDEX-0002), SFRI STRATUS project (ANR-20-SFRI-0012), and USIAS (ANR-10-IDEX-0002-02), under the framework of the French Investments for the Future Program.

Appendix A: Experimental setup and calibration

Our experimental setup consists in optically trapping, in a harmonic potential, a single dielectric bead (3 μm polystyrene sphere) in a fluidic cell filled with dionized water at room temperature $T = 296$ K. The harmonic potential is induced by focusing inside the cell a linearly polarized Gaussian beam (800 nm, CW 5 W Ti:Sa laser, Spectra Physics 3900S) through a high numerical aperture objective (Nikon Plan Apo VC, 60 \times , NA= 1.20 water immersion, Obj1 on Fig. 5). The intensity of this trapping beam is controlled by an acousto-optic modulator (Gooch and Housego 3200s, AOM on Fig. 5) using a digital-to-analogue card (NI PXIe 6361) and a PYTHON code.

The instantaneous position x_t of the sphere along the optical axis is measured by recording the light scattered off

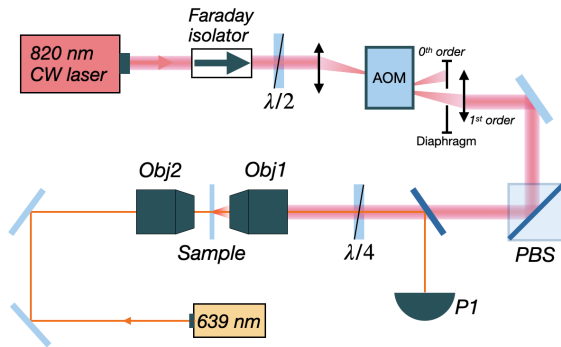


FIG. 5. Simplified view of the optical trapping setup. The sphere is suspended in water inside the *Sample* cell inserted between the two objectives Obj1 and Obj2. The 820 nm trapping beam is drawn in pink. The intensity of this beam controlled by the acousto-optic modulator (AOM). The instantaneous position of the trapped bead is probed using the auxiliary 639 nm laser beam, drawn in orange, whose scattered laser signal is sent to a high-frequency photodiode.

the sphere of a low-power 639 nm laser (CW 30 mW laser diode, Thorlabs HL6323MG), sent on the bead via a second objective (Nikon Plan Fluor Extra Large Working Distance, 60 \times , NA= 0.7, Obj2 on the figure). The scattered light is collected by Obj1 and recorded by a photodiode (100 MHz, Thorlabs Det10A). The recorded signal (in V/s) is amplified using a low noise amplifier (SR560, Stanford Research) and then acquired by an analog-to-digital card (NI PCI-6251). The signal is filtered through a 0.3 Hz high-pass filter at 6 dB/oct to remove the DC component and through a 100 kHz low-pass filter at 6 dB/oct to prevent from aliasing. The scattered intensity varies linearly with the position of the trapped bead x_t for small enough displacements and we make sure to work in the linear response regime of the photodiode so that the recorded signal is linear with the intensity, resulting in a voltage trace well linear with $x(t)$.

To build an SR process with the expected characteristics, we rely on the knowledge of the stiffness of the optical trap in which the particle diffuses. We therefore calibrate the relation between the voltage send to the AOM driver and the stiffness κ of the optical potential. On Fig. 6 (a) we show the power spectral density (PSD) of the recorded trajectories for 6 values of voltages, spanning the beginning of the dynamical bandwidth of the AOM. An issue here is that, as the stiffness increases, the motional variance of the microsphere decreases, making it harder to probe. For stiffnesses larger than circa. 40 pN/ μm we can hardly obtain a good PSD. We can however assume that the linear increase of κ with driving voltage is unaffected by this probing issue. We therefore probe the beginning of this linearity, (driving voltage from 0.01 V to 0.4 V) and extrapolate the linear relation on the whole dynamical bandwidth of the AOM, as shown Fig. 6 (b). This gives a maximal stiffness $\kappa_{\text{max}} = 83.1 \pm 2.1$ pN/ μm for the resetting event.

From the same PSD fit, we can extract a calibration factor β by the ration between the amplitude of the measured PSD in V^2/Hz and the expected value in m^2/Hz depending

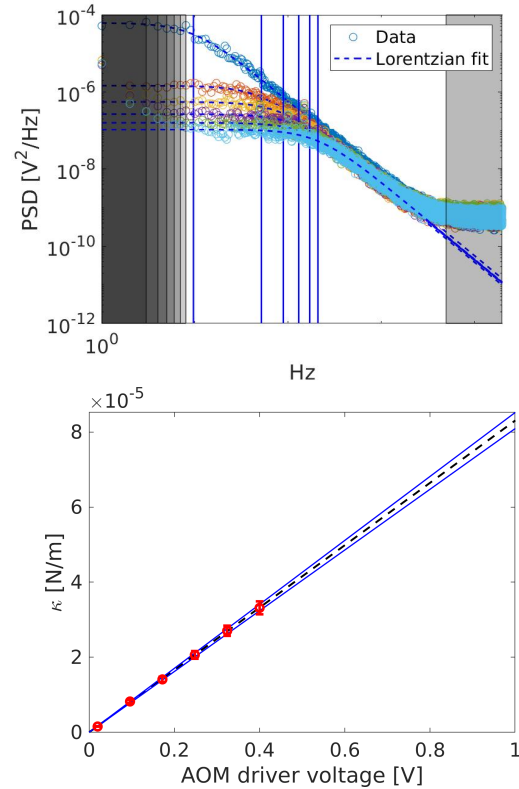


FIG. 6. (Upper panel) Power spectral density of the microsphere motion for various trapping laser intensity. The circles are experimentally measured PSD, the dashed lines are Lorentzian fits, from which the cutoff frequency is extracted (blue vertical lines). The shaded patches represent the limits of the frequencies used for the Lorentzian fit, we gradually restrain the bandwidth as we go to high stiffnesses where the measured signal decreases. (Lower panel) Stiffnesses extracted from the fit of PSDs at different driving voltage of AOM (hence different trapping laser intensity) with a linear fit giving the relation between driving voltage and in situ stiffness. This allow us to know the maximal usable stiffness given this working power (400 mW in the input of AOM) of Ti:Sap laser at $\kappa_{\text{max}} = 83.1 \pm 2.1$ pN/ μm .

on the diffusion coefficient of the microsphere in water $D = k_B T / \gamma \approx 0.16$ $\mu\text{m}^2/\text{s}$. This calibration factor allows to obtain trajectories in meter out of the recorded time-series of voltages.

On Fig. 7, we show a full time-series of recorded points (for a few milliseconds). By removing points during the waiting times (red stripes) an instantaneous resetting is event, as presented in the main text.

Appendix B: Numerical simulations

The experimental results presented in this paper are complemented by numerical simulations. In order to be

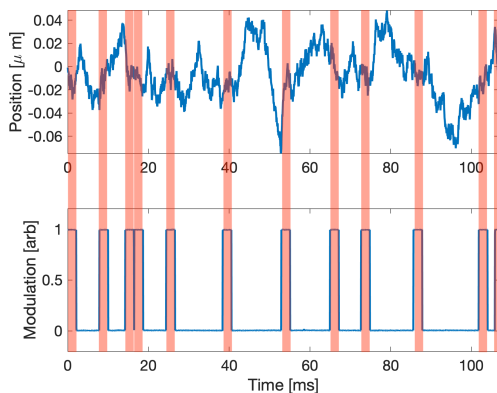


FIG. 7. Small sub-part of an experimental realization of stochastic resetting. On this figure we show the full time series of both the modulation potential and the recorded time-series. We highlight with red stripes the times when the potential is kept stiff, which corresponds to the resetting events. By removing the points during these times, one obtains an ideal instantaneous resetting process.

able to reproduce numerically both the ideal instantaneous resetting as well as the physical realization as we do with experimental data, we simulate the complete experimental scheme. Numerical SR process are, like in the experiment, solutions of Langevin equations in time-dependent external potential, which stiffness varies from κ_{\min} to κ_{\max} , both fed with experimental values. The Langevin equation is solved using a standard Euler scheme [45]. Both the random white noise simulating the thermal bath and the random distributions of times τ used to devise the resetting sequence are generated using built-in PYTHON pseudo-random number generators.

The trajectories obtained from these simulations are fully comparable to the experimental time-series and can be analyzed the same way. They are used to correct small calibration offset in the recorded trajectory, obtained by comparing the motional variance of simulated and recorded trajectories in a steady-state. This is a constant correction on calibration factor $\beta = 0.822 \beta$ that does not change the dynamics of any observed effect.

Appendix C: Ergodicity and drift correction

Ergodicity of the stochastic processes at play is evaluated with a statistical ensemble of individual sub-trajectories, drawn out of a long time-series of position x_t .

On Fig. 8 (a) we show a schematic representation of how a statistical ensemble is built out of a single time-series of position. On each individual sub-trajectory, we can compute the time-averaged mean-square-displacement (TA-MSD)

$$\text{TA-MSD} \equiv \overline{\delta_x^2}(\Delta) \equiv \frac{1}{\mathcal{T} - \Delta} \int_0^{\mathcal{T} - \Delta} (x_{t+\Delta}^i - x_t^i)^2 dt \quad (\text{C1})$$

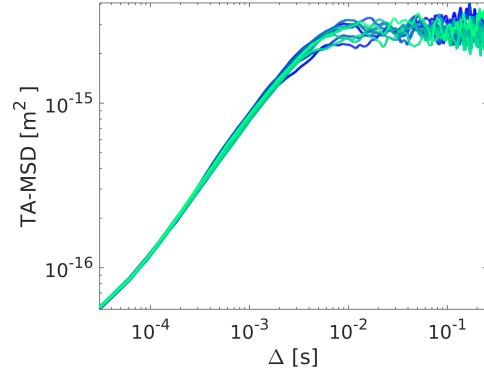
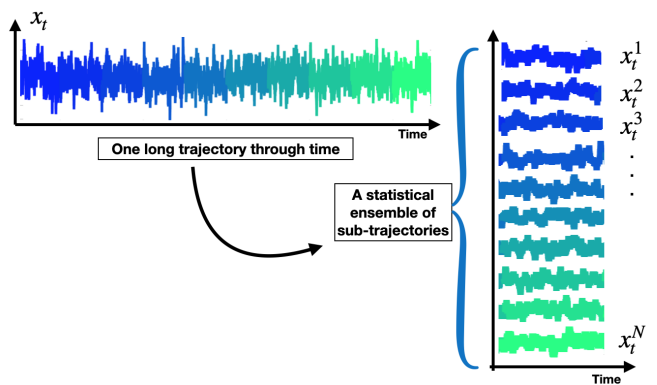


FIG. 8. (Upper panel) Schematic representation of the method used to build an ensemble out of a single long time-series of position, from a single 2.5 seconds trajectory to an ensemble of 10 individual 0.25 seconds sub-trajectories. (Lower panel) Associated 10 individual TA-MSD.

where \mathcal{T} is the total time of the measured sub-trajectory. Because of the finite size of sub-trajectories, a dispersion is still visible on the ensemble TA-MSD as seen on Fig. 8 (b). Ergodicity, as explained in the main text, is probed by looking at the evolution of this dispersion as a function of \mathcal{T}/Δ , a necessary and sufficient condition for the process to be ergodic being the vanishing of the dispersion for short Δ . However, if the experimental setup suffers from low frequency drift on the 300-seconds long experiments, this dispersion will be combined with a systematic trend, that will lead to an overestimation of the ergodic parameter $\epsilon(\Delta) \sim \text{var}(\text{TA-MSD})$. In this Appendix, we propose a novel method to decipher systematic from statistic dispersion of TA-MSD, by relying on their very short-time limit. This allows to correct drifts and clearly unveil the different between ergodic normal Brownian motion in a potential from non-ergodic SR process.

We consider here, as in the section of the main text focused on Landauer's limit, a 300 second long trajectory that can be recast into an ensemble of a thousand sub-trajectories of 0.3 seconds each, diffusing in an optical potential of stiffness $\kappa_{\min} = 2.9 \pm 0.15$ pN/ μm . We study both a normal Brownian motion diffusing in the aforementioned potential as well as an SR process in the same potential, but in which

the optical potential is increased to $\kappa_{\max} \approx 83$ pN/ μm at a rate $\lambda^{-1} = 20 \omega_{\max}^{-1} \approx 6.1$ ms. Each TA-MSD is computed as a time integral on individual sub-trajectories of total time $\mathcal{T} = 0.3$ seconds. By comparing TA-MSDs at different absolute times, we can detect low frequency drifts. To achieve the best accuracy, we probe TA-MSD for very short time-lag $\Delta = 0.061$ ms where the statistical dispersion of TA-MSD is the smallest.

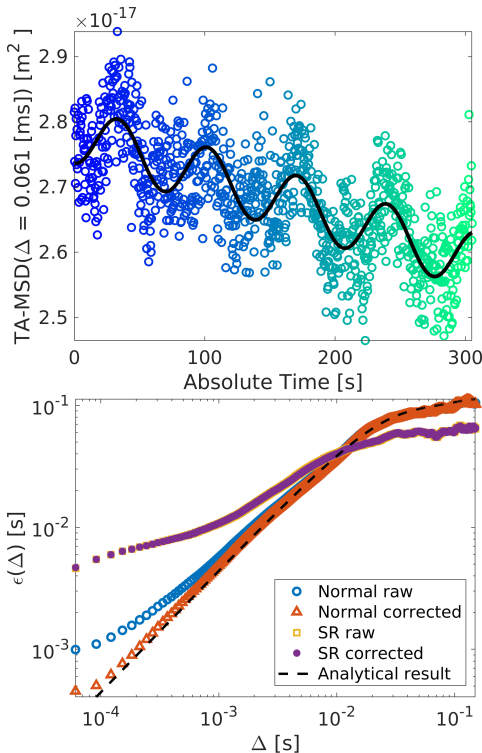


FIG. 9. (Upper panel) Short time-lag TA-MSD $\overline{\delta_{x_i}^2}(\Delta = 0.061[\text{ms}])$ for each individual chronologically ordered sub-trajectories as a function of the absolute time in seconds. We clearly observe a systematic trend, that is well captured by the combination of linear decrease and a ≈ 10 s sinusoidal evolution. The magnitude of the drift is of the order of 1.4 nm of mean displacement. (Lower panel) Associated ergodic parameter, both for a normal Brownian motion in a potential of stiffness κ_{\min} and for an SR process in the same potential. We show the raw data measured from the calibrated photodiode as well as the same observable on data where the 1.4 nm mean displacement drift on the 300 s has been corrected.

On Fig. 9 (a) we show the value of TA-MSD at $\Delta = 0.061$ ms from blue to green for each chronologically ordered sub-trajectory as a function of the absolute time of the experiment. It corresponds to a vertical cut in a TA-MSD plot such as displayed Fig. 8 (b). We can observe, superimposed to the expected dispersion a systematic trend. We fit the behaviour with a guess function, combination of negative constant slope and a 10 second sinusoidal oscillation. The fit gives the black continuous line on Fig. 9 (a) and is used to correct as a function of time the calibration factor used to convert the measured voltages into meter.

On both the raw measured data and the data corrected with the aforementioned method, we compute the ergodic parameter $\epsilon(\Delta)$ probing the dispersion of TA-MSD as a function of lag-time Δ . On Fig. 9 (b) we show the effect of drift correction. We show the ergodic parameter $\epsilon(\Delta)$ for a normal Brownian without correction (blue circles) and with calibration correction (red triangles). Remarkably, the minute correction fitted on the short time-limit of TA-MSD very neatly recast the ergodic parameter on the expected analytical result (black dashed line), computed for a Brownian motion in a potential of stiffness $\kappa = 83$ pN/ μm . This proves that the short time-lag deviation of ϵ for normal Brownian motion is solely due to drift and not to a physical ergodicity breaking. On the other hand the ergodic parameter evaluated on the SR process is strongly departing from this trend and does not vanishes for short Δ . Furthermore, the magnitudes of ϵ probed are significantly larger and are therefore not affected by the drift (the statistical dispersion of TA-MSD is larger than the systematic trend) as seen in the equality of the ergodic parameter for the raw data (yellow squares) and corrected data (purple stars). This assesses the validity of the test: the deviation for SR process is not due to a drift, but to a physical ergodicity breaking.

Appendix D: Stationary distributions

Trapped Brownian trajectories undergoing an SR process are distributed according to a steady-state probability distribution function that depends both on the confining potential and the resetting parameters. In our case, the Brownian microsphere is optically trapped in a locally harmonic potential $V(x) = \frac{1}{2}\kappa_{\min}x^2$, where $\kappa_{\min} \sim 10^{-6}$ N/m is the stiffness of the confining potential (in contrast with $\kappa_{\max} \sim 10^{-4}$ N/m which corresponds to the potential quench associated with each resetting event). This confining potential, together with the viscous drag γ experienced by the microsphere in the fluid, induces a characteristic pulsation $\omega_0 = \kappa_{\min}/\gamma \sim 10^{-3}$ s in the dynamics.

The steady state solution for the Fokker Planck equation with stochastic resetting is [18]

$$P(x) = \lambda \int_0^\infty d\tau e^{-\lambda\tau} G(x|\tau, 0), \quad (\text{D1})$$

where λ is the rate of the Poissonian stochastic resetting and $G(x|\tau, 0)$ is the propagator of a given stochastic process that is reset to. For a Wiener process, the propagator is

$$G(x|\tau, 0) = \frac{1}{\sqrt{4\pi D\tau}} \exp\left(-\frac{x^2}{4D\tau}\right). \quad (\text{D2})$$

Therefore, the corresponding integral to solve is

$$P(x) = \frac{\lambda}{\sqrt{4\pi D}} \int_0^\infty \frac{d\tau}{\sqrt{\tau}} \exp\left[-\left(\lambda\tau + \frac{x^2}{4D\tau}\right)\right] \quad (\text{D3})$$

now, let $u = \sqrt{\tau}$, the integral becomes then

$$\begin{aligned} P(x) &= \frac{\lambda}{\sqrt{\pi D}} \int_0^\infty du \exp\left(-\lambda u^2 - \frac{x^2}{4Du^2}\right) \\ &= \frac{1}{2} \sqrt{\frac{\lambda}{D}} \exp\left(-\sqrt{\frac{\lambda}{D}} |x|\right). \end{aligned} \quad (\text{D4})$$

This corresponds to an exponential distribution.

For a Ornstein-Uhlenbeck process, the propagator is given by

$$G(x|\tau, 0) = \sqrt{\frac{\omega_0}{2\pi D(1 - e^{-2\omega_0\tau})}} \exp\left(-\frac{\omega_0}{2D} \cdot \frac{x^2}{1 - e^{-2\omega_0\tau}}\right), \quad (\text{D5})$$

where the parameter $\omega_0 = \kappa/\gamma$. For simplicity, we define $a = \omega_0/2D$ and $b = 2\omega_0$. Thus, the steady state PDF can be written as

$$P(x) = \sqrt{\frac{a}{\pi}} \int_0^\infty d\tau r e^{-\lambda\tau} \frac{1}{\sqrt{1 - e^{-b\tau}}} \exp\left(-\frac{ax^2}{1 - e^{-b\tau}}\right). \quad (\text{D6})$$

Applying the change of variable $u = e^{-\lambda\tau}$ leads to $e^{-b\tau} = u^p$ where $p = b/\lambda$. The integral thus becomes

$$P(x) = \sqrt{\frac{a}{\pi}} \int_0^1 du \frac{1}{\sqrt{1 - u^p}} \exp\left(-\frac{ax^2}{1 - u^p}\right). \quad (\text{D7})$$

A second change of variable defined by $w = 1 - u^p$, where $du = -\frac{1}{p}(1 - w)^{\frac{1}{p}-1} dw$, gives the expression for the probability distribution

$$P(x) = \sqrt{\frac{a}{\pi}} \int_0^1 dw \frac{1}{p} (1 - w)^{\frac{1}{p}-1} w^{-1/2} \exp\left(-\frac{ax^2}{w}\right). \quad (\text{D8})$$

According to Gradshteyn & Ryzhik 3.471.2 [46], our integral leads to the final result:

$$P(x) = \frac{1}{p} \sqrt{\frac{a}{\pi}} \Gamma\left(\frac{1}{p}\right) e^{-\frac{ax^2}{2}} (ax^2)^{-\frac{1}{4}} W_{\frac{1}{4}-\frac{1}{p}, \frac{1}{4}}(ax^2), \quad (\text{D9})$$

where $W_{k,m}(x)$ is the Whittaker function.

The result Eq. (D9) is used in the main text and agrees with the experimentally measured distribution for an SR process

in a harmonic potential. This agreement validates our experimental realization of SR. On Fig. 10, we show the agreement between experimentally measured steady-state distributions and the result Eq. (D9) for various resetting rates, ranging from 283 to 795 Hz. The analytical expression captures the experimental behavior on a large spacial range as well as on an extended parameter variation. One can note that the steady-states share a sharp central peak, similar to the exponential distribution of *free* SR process, while the tails tends to follow the (Ornstein-Uhlenbeck) Gaussian tails. For small λ/ω_0 , the distribution is closer to the Gaussian corresponding to a trajectory without resetting while the distribution is progressively more sharply peaked around the resetting position $x = 0$ when the resetting rate increases, departing more strongly from the Gaussian distribution.

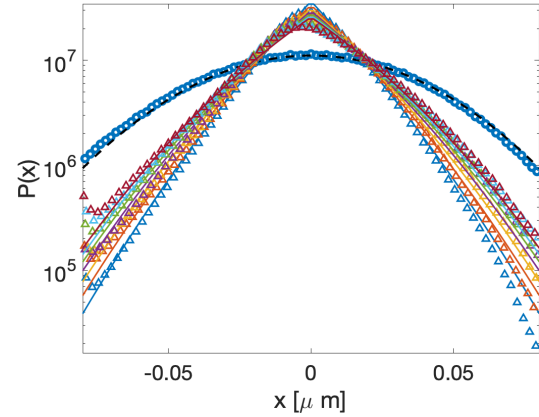


FIG. 10. Experimental histograms (triangles) together with the exact distribution Eq. (D9) (solid lines) for a large range of resetting rates from $\lambda = 283$ Hz to $\lambda = 795$ Hz while $\omega_0 = 159$ Hz. As a comparison, the Gaussian probability distribution of a Brownian trajectory in the same potential $V(x)$ with the characteristic pulsation ω_0 is shown (black dashed line) together with the associated experimentally measured histogram (blue circles).

Importantly, this result generalizes the expression known in the literature for SR in a harmonic potential. This expression is expressed in terms of negative order Hermite's polynomials [33, 47]. Indeed, if the two results coincides exactly for integer values of λ/ω_0 , our result, based on the Whittaker function is not restricted to integer ratio between the resetting rate and the characteristic pulsation, since the parameter k and m of $W_{k,m}(x)$ function can take arbitrary real values.

-
- [1] M. R. Evans and S. N. Majumdar, Diffusion with stochastic resetting, *Phys. Rev. Lett.* **106**, 160601 (2011).
 [2] J. Fuchs, S. Goldt, and U. Seifert, Stochastic thermodynamics of resetting, *EPL (Europhysics Letters)* **113**, 60009 (2016).
 [3] É. Roldán, I. A. Martínez, J. M. R. Parrondo, and D. Petrov, Universal features in the energetics of symmetry breaking, *Nature Physics* **10**, 457 (2014).
 [4] S. Ciliberto and E. Lutz, The physics of information: From

- maxwell to landauer (Springer International Publishing, Cham, 2019) pp. 155–175.
 [5] E. Lutz and S. Ciliberto, Information: From maxwell's demon to landauer's eraser, *Physics Today* **68**, 30 (2015), <https://doi.org/10.1063/PT.3.2912>.
 [6] S. C. Manrubia and D. H. Zanette, Stochastic multiplicative processes with reset events, *Phys. Rev. E* **59**, 4945 (1999).
 [7] A. Chechkin and I. M. Sokolov, Random search with reset-

- ting: A unified renewal approach, *Phys. Rev. Lett.* **121**, 050601 (2018).
- [8] M. R. Evans, S. N. Majumdar, and G. Schehr, Stochastic resetting and applications, *Journal of Physics A: Mathematical and Theoretical* **53**, 193001 (2020).
- [9] A. Stanislavsky and A. Weron, Optimal non-gaussian search with stochastic resetting, *Phys. Rev. E* **104**, 014125 (2021).
- [10] E. Roldán, A. Lisica, D. Sánchez-Taltavull, and S. W. Grill, Stochastic resetting in backtrack recovery by rna polymerases, *Phys. Rev. E* **93**, 062411 (2016).
- [11] P. C. Bressloff, Modeling active cellular transport as a directed search process with stochastic resetting and delays, *Journal of Physics A: Mathematical and Theoretical* **53**, 355001 (2020).
- [12] O. Blumer, S. Reuveni, and B. Hirshberg, Stochastic resetting for enhanced sampling, *The Journal of Physical Chemistry Letters* , 11230 (2022).
- [13] M. R. E. S. N. M. John C. Sunil, Richard A. Blythe, The cost of stochastic resetting, Arxiv [arXiv:2304.09348](https://arxiv.org/abs/2304.09348) (2023).
- [14] D. Gupta, C. A. Plata, and A. Pal, Work fluctuations and Jarzynski equality in stochastic resetting, *Phys. Rev. Lett.* **124**, 110608 (2020).
- [15] A. Pal, S. Reuveni, and S. Rahav, Thermodynamic uncertainty relation for systems with unidirectional transitions, *Phys. Rev. Research* **3**, 013273 (2021).
- [16] S. Gupta and A. M. Jayannavar, Stochastic resetting: A (very) brief review, *Frontiers in Physics* **10**, 10.3389/fphy.2022.789097 (2022).
- [17] D. Gupta and C. A. Plata, Work fluctuations for diffusion dynamics submitted to stochastic return, *New Journal of Physics* **24**, 113034 (2022).
- [18] F. Mori, K. S. Olsen, and S. Krishnamurthy, Entropy production of resetting processes, *Phys. Rev. Res.* **5**, 023103 (2023).
- [19] M. Esposito and C. V. den Broeck, Second law and Landauer principle far from equilibrium, *EPL (Europhysics Letters)* **95**, 40004 (2011).
- [20] V. Stojkoski, T. Sandev, L. Kocarev, and A. Pal, Geometric brownian motion under stochastic resetting: A stationary yet nonergodic process, *Phys. Rev. E* **104**, 014121 (2021).
- [21] W. Wang, A. G. Cherstvy, H. Kantz, R. Metzler, and I. M. Sokolov, Time averaging and emerging nonergodicity upon resetting of fractional brownian motion and heterogeneous diffusion processes, *Phys. Rev. E* **104**, 024105 (2021).
- [22] V. Stojkoski, T. Sandev, L. Kocarev, and A. Pal, Autocorrelation functions and ergodicity in diffusion with stochastic resetting, *Journal of Physics A: Mathematical and Theoretical* **55**, 104003 (2022).
- [23] O. Tal-Friedman, A. Pal, A. Sekhon, S. Reuveni, and Y. Roichman, Experimental realization of diffusion with stochastic resetting, *The Journal of Physical Chemistry Letters* **11**, 7350 (2020).
- [24] B. Besga, A. Bovon, A. Petrosyan, S. N. Majumdar, and S. Ciliberto, Optimal mean first-passage time for a brownian searcher subjected to resetting: Experimental and theoretical results, *Phys. Rev. Research* **2**, 032029 (2020).
- [25] I. Santra, S. Das, and S. K. Nath, Brownian motion under intermittent harmonic potentials, *Journal of Physics A: Mathematical and Theoretical* **54**, 334001 (2021).
- [26] B. Besga, F. Faisant, A. Petrosyan, S. Ciliberto, and S. N. Majumdar, Dynamical phase transition in the first-passage probability of a brownian motion, *Phys. Rev. E* **104**, L012102 (2021).
- [27] K. Sekimoto, Langevin Equation and Thermodynamics, *Progress of Theoretical Physics Supplement* **130**, 17 (1998), <https://academic.oup.com/ptps/article-pdf/doi/10.1143/PTPS.130.17/5213518/130-17.pdf>.
- [28] D. Gupta, C. A. Plata, A. Kundu, and A. Pal, Stochastic resetting with stochastic returns using external trap, *Journal of Physics A: Mathematical and Theoretical* **54**, 025003 (2020).
- [29] A. S. Bodrova and I. M. Sokolov, Resetting processes with non-instantaneous return, *Phys. Rev. E* **101**, 052130 (2020).
- [30] G. Mercado-Vásquez, D. Boyer, S. N. Majumdar, and G. Schehr, Intermittent resetting potentials, *Journal of Statistical Mechanics: Theory and Experiment* **2020**, 113203 (2020).
- [31] I. M. Sokolov, Linear response and fluctuation-dissipation relations for brownian motion under resetting, *Phys. Rev. Lett.* **130**, 067101 (2023).
- [32] Note that a finite value of κ_{\max} induces a small error on the resetting position. However, this error does not affect the distribution, as seen from the very good agreement between the experimental steady-state and the exact result.
- [33] A. Pal, Diffusion in a potential landscape with stochastic resetting, *Phys. Rev. E* **91**, 012113 (2015).
- [34] U. Seifert, Entropy production along a stochastic trajectory and an integral fluctuation theorem, *Phys. Rev. Lett.* **95**, 040602 (2005).
- [35] D. M. Busiello, D. Gupta, and A. Maritan, Entropy production in systems with unidirectional transitions, *Phys. Rev. Research* **2**, 023011 (2020).
- [36] A. Bérut, A. Arakelyan, A. Petrosyan, S. Ciliberto, R. Dillenschneider, and E. Lutz, Experimental verification of Landauer's principle linking information and thermodynamics, *Nature* **483**, 187 (2012).
- [37] Y. Jun, M. c. v. Gavrilo, and J. Bechhoefer, High-precision test of Landauer's principle in a feedback trap, *Phys. Rev. Lett.* **113**, 190601 (2014).
- [38] J. M. R. Parrondo, J. M. Horowitz, and T. Sagawa, Thermodynamics of information, *Nature Physics* **11**, 131 (2015).
- [39] M. R. Evans, S. N. Majumdar, and K. Mallick, Optimal diffusive search: nonequilibrium resetting versus equilibrium dynamics, *Journal of Physics A: Mathematical and Theoretical* **46**, 185001 (2013).
- [40] R. Metzler and J. Klafter, The random walk's guide to anomalous diffusion: a fractional dynamics approach, *Physics Reports* **339**, 1 (2000).
- [41] A. G. Cherstvy and R. Metzler, Ergodicity breaking, ageing, and confinement in generalized diffusion processes with position and time dependent diffusivity, *J. Stat. Mech.* **2015**, P05010 (2015).
- [42] M. Li, O. Sentissi, S. Azzini, G. Schnoering, A. Canaguier-Durand, and C. Genet, Subfemtonewton force fields measured with ergodic brownian ensembles, *Phys. Rev. A* **100**, 063816 (2019).
- [43] R. Goerlich, M. Li, S. Albert, G. Manfredi, P.-A. Hervieux, and C. Genet, Noise and ergodic properties of brownian motion in an optical tweezer: Looking at regime crossovers in an Ornstein-Uhlenbeck process, *Phys. Rev. E* **103**, 032132 (2021).
- [44] R. Metzler, J.-H. Jeon, A. G. Cherstvy, and E. Barkai, Anomalous diffusion models and their properties: non-stationarity, non-ergodicity, and ageing at the centenary of single particle tracking, *Phys. Chem. Chem. Phys.* **16**, 24128 (2014).
- [45] G. Volpe and G. Volpe, Simulation of a Brownian particle in an optical trap, *Am. J. Phys.* **81**, 224 (2013), <https://doi.org/10.1119/1.4772632>.
- [46] I. S. Gradshteyn and I. M. Ryzhik, *Table of integrals, series, and products*, seventh ed. (Elsevier/Academic Press, Amsterdam, 2007) pp. xlviii+1171, translated from the Russian, Translation edited and with a preface by Alan Jeffrey and Daniel Zwillinger, With one CD-ROM (Windows, Macintosh and UNIX).

[47] P. Trajanovski, P. Jolakoski, K. Zelenkovski, A. Iomin, L. Kocarev, and T. Sandev, Ornstein-uhlenbeck process and gen-

eralizations: Particle dynamics under comb constraints and stochastic resetting, [Phys. Rev. E **107**, 054129 \(2023\)](#).